Solar Energy 175 (2018) 68–74

Contents lists available at ScienceDirect

Solar Energy

journal homepage: www.elsevier.com/locate/solener

High-performance p-type multicrystalline silicon (mc-Si): Its characterization and projected performance in PERC solar cells

Pietro P. Altermatt[a], Zhen Xiong[a], QiuXiang He[a], WeiWei Deng[a], Feng Ye[a], Yang Yang[a], Yifeng Chen[a], ZhiQiang Feng[a], Pierre J. Verlinden[a,*], Anyao Liu[b], Daniel H. Macdonald[b], Tabea Luka[c], Dominik Lausch[c], Marko Turek[c], Christian Hagendorf[c], Hannes Wagner-Mohnsen[d], Jonas Schön[e], Wolfram Kwapil[e], Felix Frühauf[f], Otwin Breitenstein[f], Erin E. Looney[g], Tonio Buonassisi[g], David B. Needleman[g,1], Christine M. Jackson[h], Aaron R. Arehart[h], Steven A. Ringel[h], Keith R. McIntosh[i], Malcolm D. Abbott[i], Ben A. Sudbury[i], Annika Zuschlag[j], Clemens Winter[j], Daniel Skorka[j], Giso Hahn[j], Daniel Chung[k], Bernhard Mitchell[k], Peter Geelan-Small[k], Thorsten Trupke[k]

[a] Trina Solar, State Key Laboratory for Photovoltaic Science and Technology (SKL PVST), Xinbei District, Changzhou, Jiangsu Province 213031, China
[b] Research School of Engineering, The Australian National University, Canberra 2601 ACT, Australia
[c] Fraunhofer Center for Silicon Photovoltaics CSP, O.-Eissfeldt-Str. 12, D-06120 Halle, Germany
[d] Global Photovoltaic Simulation Group, Case Postale 1056, 1211 Genève 1, Switzerland
[e] Fraunhofer Institute for Solar Energy Systems, Heidenhofstraße 2, D-79110 Freiburg, Germany
[f] Max Planck Institute of Microstructure Physics, Weinberg 2, 06120 Halle (Saale), Germany
[g] Mechanical Engineering Dep., Massachusetts Institute of Technology, Cambridge, MA 02139, USA
[h] Dep. of Electrical and Computer Engineering, The Ohio State University, Columbus, OH 43210, USA
[i] PV Lighthouse, Coledale, NSW 2515, Australia
[j] University of Konstanz, Department of Physics, 78457 Konstanz, Germany
[k] School of Photovoltaic and Renewable Energy Engineering, UNSW, Sydney, NSW 2052, Australia

ARTICLE INFO

Keywords:
Multicrystalline silicon
Ingot metrology
Cell characterization
Excess carrier lifetime
PERC cells
Modeling

ABSTRACT

Recent progress in the electronic quality of high-performance (HP) multicrystalline silicon material is reported with measurements and modeling performed at various institutions and research groups. It is shown that recent progress has been made in the fabrication at Trina Solar mainly by improving the high excess carrier lifetimes τ due to a considerable reduction of mid-gap states. However, the high lifetimes in the wafers are still reduced by interstitial iron by a factor of about 10 at maximum power point (mpp) conditions compared to mono-crystalline Cz wafers of equivalent resistivity. The low lifetime areas of the wafers seem to be limited by precipitates, most likely Cu. Through simulations, it appears that dislocations reduce cell efficiency by about 0.25% absolute. The best predictors for PERC cell efficiency from ingot metrology are a combination of mean lifetime and dislocation density because dislocations cannot be improved considerably by gettering during cell processing, while lifetime-limiting impurities are gettered well. In future, the material may limit cell efficiency above about 22.5% if the concentrations of Fe and Cu remain above 10^{10} and $10^{13}\,cm^{-3}$, respectively, and if dislocations are not reduced further.

1. Introduction

For decades, multicrystalline silicon (mc-Si) has been widely used for the production of solar cells. Improving the material has been complex yet progressive because characterization methods for this material have been greatly improved. In this paper, lifetime-limiting phenomena are quantified in material produced at Trina Solar by in-depth characterization, using specialized equipment in various research groups, and by modeling. The impact of lifetime on PERC cell efficiency is investigated and, from that, the behavior of the material and its

* Corresponding author.
E-mail address: pierre.verlinden@trinasolar.com (P.J. Verlinden).
[1] Now with: OneSun Solar, Berkeley, CA 94710, USA.

https://doi.org/10.1016/j.solener.2018.01.073
Received 4 November 2017; Accepted 21 January 2018
Available online 14 February 2018
0038-092X/

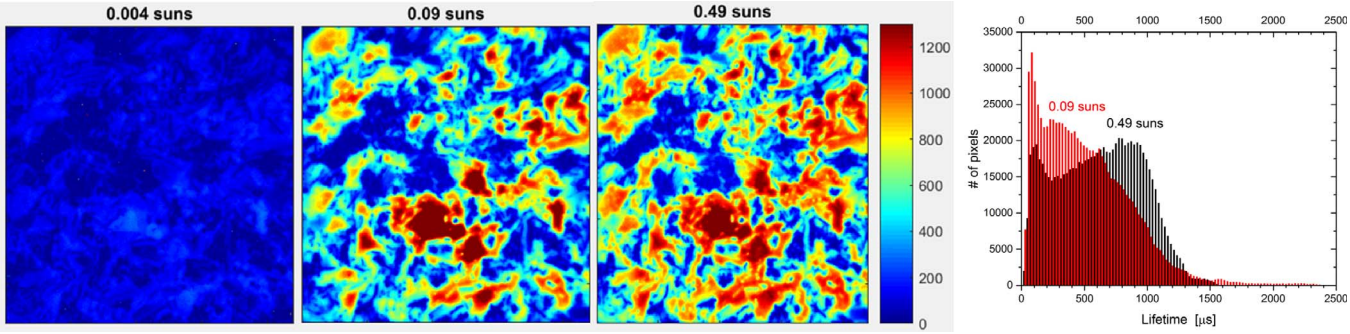

Fig. 1. Photoluminescence lifetime images (in µs) at the indicated light intensities of 15.6 × 15.6 cm^2 wafers, fabricated at Trina Solar, then phosphorus gettered, passivated with Al_2O_3, and measured at the Australian National University. Right: histogram of the PL camera pixels.

requirements along the PERC roadmap are forecast.

2. Assessing the quality of multi Si wafers

Fig. 1 shows photoluminescence images obtained at various light intensities, measured with a combination of photoluminescence (PL) and quasi-steady state photo-conductance (QSSPC) and applying a data evaluation procedure described in reference Sio et al. (2014). This investigation at the Australian National University (ANU) quantified how the lifetimes are mostly injection-dependent (as usual in multi material), meaning that they increase with illumination intensity or local injection density Δn. The histogram of PL camera pixels shows that the distribution moves towards lower lifetimes at lower light intensities. As a rule of thumb, PL is performed at a light intensity of about 0.1 suns to mimic the injection condition at the maximum power point (mpp), because – in homogeneous material – Δn is about 10-fold reduced compared to the open-circuit condition (from slightly above $10^{15}\,cm^{-3}$ to slightly below $10^{14}\,cm^{-3}$, depending on the quality of the cell).

In order to obtain an understanding of the lifetime, it is instructive to fit 1% of the best lifetimes of Fig. 1 with the SRH theory, as shown in Fig. 2. Shockley-Read-Hall (SRH) theory never uniquely identifies defect species. However, we know that the material is contaminated with iron so it is rather straight forward to see that a concentration of about $3 \times 10^{10}\,cm^{-3}$ of Fe_i reduces these best lifetimes by a factor of about 10 at mpp conditions. If their concentration was reduced to about $2 \times 10^{9}\,cm^{-3}$, these best lifetimes would be as good as state-of-the art deactivated Czochralski (Cz) material Walter et al., 2016 at mpp conditions.

The 10% of lowest lifetimes in a non-gettered wafer is also shown at the bottom of Fig. 2 and can be described by SRH theory if assuming precipitation e.g. by Cu. A parameterization (Kwapil et al., 2015) is used at Fraunhofer ISE that they derived from process and electrical modeling. Depending on the radius of these precipitates, either the average Cu concentration can be used as input to the SRH theory (which is $5 \times 10^{13}\,cm^{-3}$, measured in non-gettered material with ICP-MS), or alternatively a higher Cu concentration ($3 \times 10^{14}\,cm^{-3}$) can be used, caused by segregation towards dislocation clusters. Note that these assumptions influence the steepness of the lifetime curve.

Fig. 3 shows the injection dependence of lifetime monitored at nearly all PL camera pixels (811'000 pixels, as only the pixels very close to the perimeter were removed). A kernel density estimate (using the software 'R' and its package 'kr') indicates the distribution of these dots: e.g. the 75% line means that 75% of all pixels are contained within the center region. The black curve then indicates the most likely injection dependence, which is quantified by SRH theory using a capture cross-section ratio of 10 if a single defect level near mid-gap is assumed. Note how narrow the dots are centered around that line. This is important input for numerical device simulations discussed in later sections of this

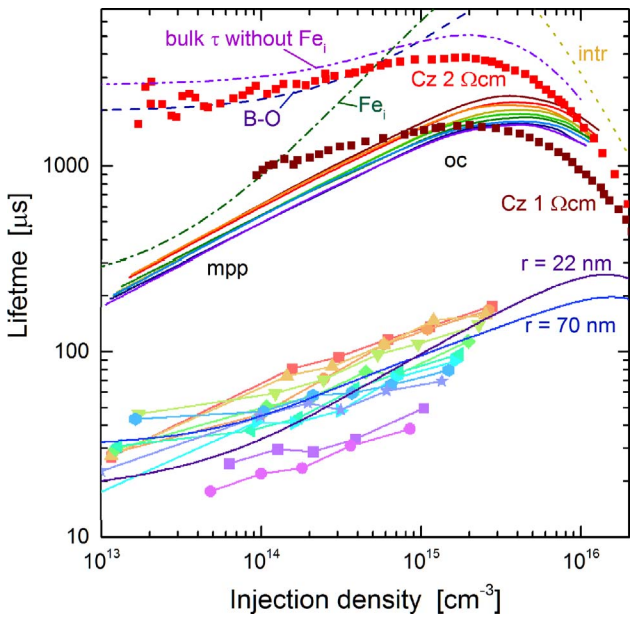

Fig. 2. Solid rainbow lines near top: every 1000th pixel within the highest 1% of lifetimes of Fig. 1. Dashed lines: contributions of interstitial iron (Fe_i), the B-O complex, and the intrinsic lifetime to a SRH fit of the highest lifetime. Also, the bulk lifetime is shown for the case if Fe were removed and is compared to lifetimes in state-of-the art deactivated Cz material (symbols) Walter et al., 2016. Lines with symbols near the bottom: every 5000th pixel of the lowest 10% of lifetimes of an ungettered wafer, described with SRH theory using Cu precipitates having the indicated radius, from ISE Freiburg.

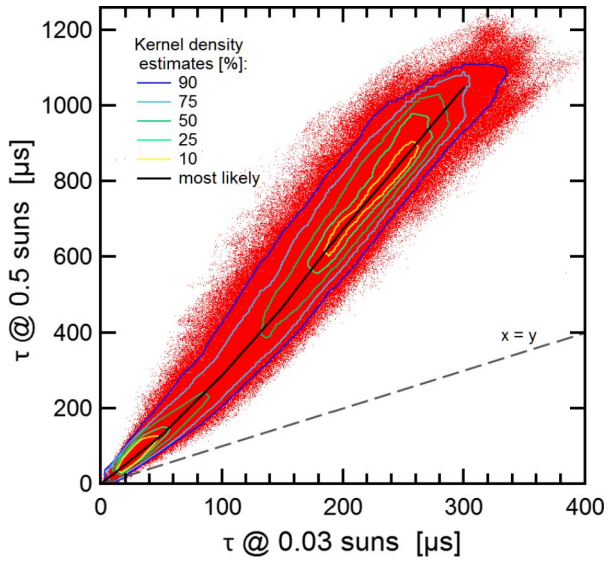

Fig. 3. 811'000 pixels of a PL image (without perimeter) at two different light intensities, and a kernel density estimate, indicating a SRH capture cross-section ratio of 10.

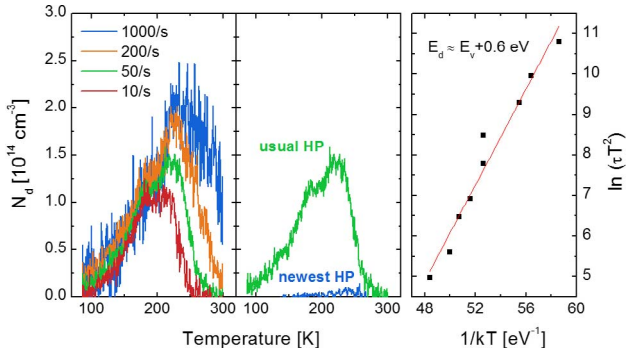

Fig. 4. DLTS measurements done at OSU at Trina material: ususal HP multi with various time constants (left), comparison of usual with newest material (middle), and extracted dominating defect energy (right).

paper.

DLTS measurements were performed at the Ohio State University (OSU) on pieces of this material, having a NiSi/Ag ohmic contact at the rear and a patterned 0.084 mm^2 Pt Schottky contact at the front surface. Fig. 4 shows the measurements with various time constants, the extraction of the dominating defect energy within the band gap, and a comparison between usual and recent high-performance (HP) material. The mid-gap states dominate and are greatly reduced in recent samples.

Considering this reduction in defects, one might argue whether p-type or n-type doping is better suited for obtaining high lifetimes. Common thought is that many metal impurities induce donor-like defects and therefore are more active inp-type than in n-type. See for example reference Schmidt et al. (2013), Fig. 5 therein. However, if Fe_i is removed effectively, the most common remaining impurities (Cu, Ni, Co, Cr) in that figure are all less active in p-type than in n-type. This may favor p-type also in the coming near future.

Overall, when SRH theory is compared to the measured Cz lifetimes in Fig. 2, it indicates that the lifetime is limited by the boron-oxygen (B-O) complex if the metal impurity concentrations are smaller than listed in Table 1. This may be achieved mainly by using cleaner nitride material for crucible coating, by storing the coated crucibles in significantly cleaner environments, and by generally cleaner material processing. Cleaner is meant here as absence of metal impurities (which are usually invisible to the naked eye), not as the absence of high-purity Si dust and abrasives (which look 'dirty').

Besides metal impurities, dislocations are known to reduce lifetime as well. See reference Needleman et al. (2016) for a Sentaurus Device

Table 1
Metal impurity concentrations such that the B-O complex limits lifetime in 1–2 Ω cm Si multi material.

Metal impurity	Concentration [cm^{-3}]
W, Co, Cr	$< 1 \times 10^9$
Fe_i, W	$< 2 \times 10^9$
Ni	$< 1 \times 10^{11}$
Cu	$< 5 \times 10^{12}$

model established at the Massachusetts Institute of Technology (MIT) on experimental findings. It predicts that Trina's recent world record efficiency multi cell would have an efficiency of 21.51% without dislocations instead of the measured 21.25% (Deng et al., 2016). Hence, dislocations presently seem to reduce cell efficiency by about 0.25% absolute. The efficiency is mainly affected by changes in J_{sc}, not so much by V_{oc}, because there is greater charging (due to majority carrier occupation) of defects at the dislocations at J_{sc} than at V_{oc} (lower injection level).

Finally, lifetime is also affected by light-induced degradation and regeneration. Fig. 5 shows the degradation and regeneration of the open-circuit voltage V_{oc}, measured at CSP Fraunhofer on multi PERC cells from Trina Solar. The degradation is both enhanced and accelerated at 130 °C and 1-sun illumination using an LED-based light-soaking test station. It behaves as it is expected from HP material; for example it depends on the position of the ingot because other defect species influence the rates of the defect reactions. There are also lateral deviations caused by crystal defects such as grain boundaries (Luka et al., 2016). As usual, the rates of regeneration are considerably slower than in monocrystalline material. This can also be seen with time-resolved PL measurements from the University of Konstanz, Fig. 6, where each line represents the evolution of lifetime of one pixel and is color-coded according to its initial lifetime. The final decline in lifetime towards 1000 h is caused by degradation of the SiN_x passivation (Sperber et al., 2017), as can be seen in lifetimes of float-zone material shown in the background of Fig. 6. Most lifetimes develop in a parallel manner. In multi cells in the field, V_{oc} usually degrades only by about 2–3 mV because, below about 80 °C, the rate of regeneration is larger than the rate of degradation (Herguth and Wilking, 2017). However, there are complexities in this simple argument, which depend on the material, its thermal history, and the geographical location, causing intense ongoing research in degradation and regeneration.

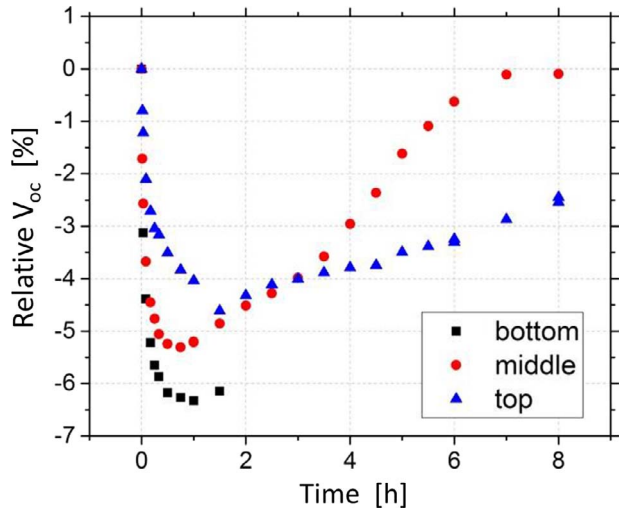

Fig. 5. Accellerated and enhanced degradation and regeneration of the open-circuit voltage V_{oc}, measured at CSP Fraunhofer on multi PERC cells from Trina Solar.

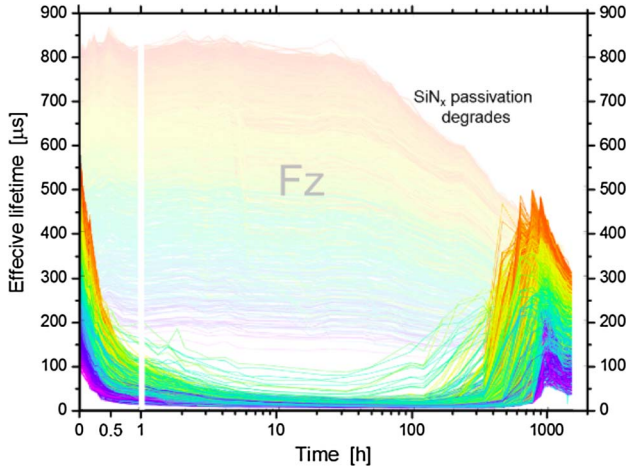

Fig. 6. Time-resolved PL measurements from the University of Konstanz at Trina HP multi material, subjected to 75 °C and 0.9 suns after phosphorus-gettering and firing in a belt furnace. Each pixel is color-coded according to its initial lifetime. Background: stability of SiN_x passivation measured in Fz material.

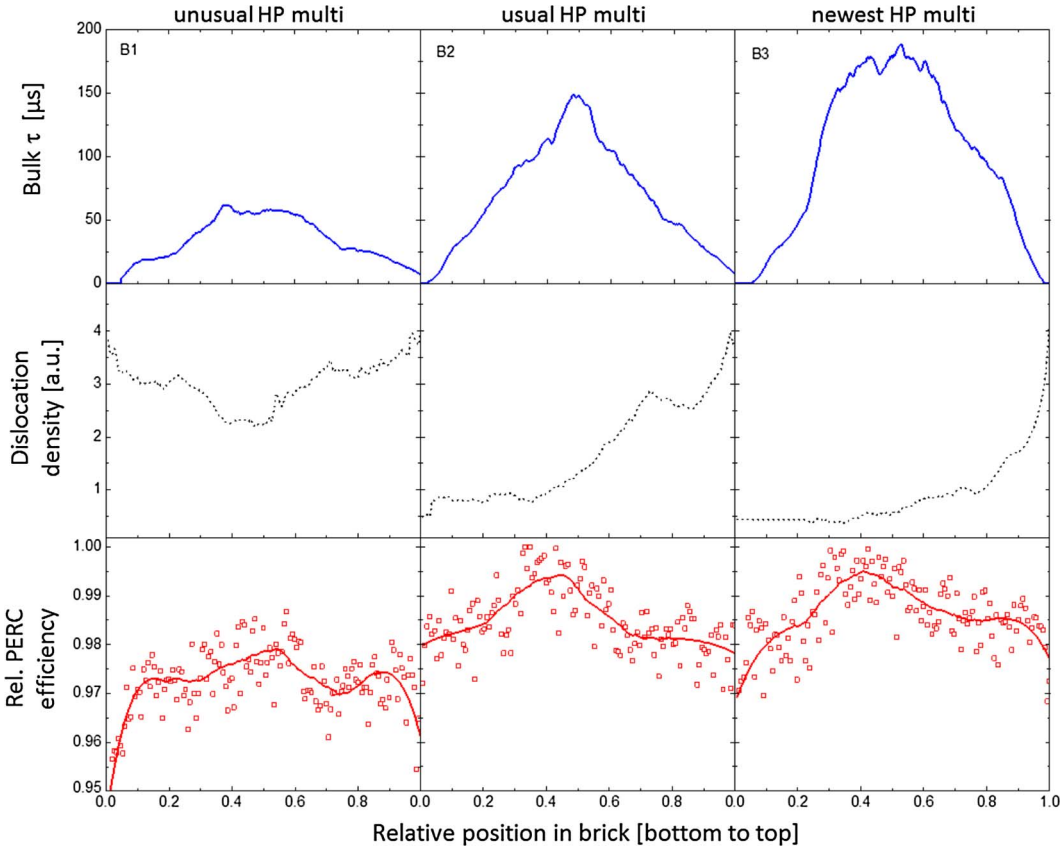

Fig. 7. Top: lifetime extracted from bricks of Trina Solar. Middle: Dislocation density parameter extracted from the image processing algirithm of the LIS-B3 tool of BT imaging. Bottom: PERC cell efficiency of cells fabricated at Trina with the same bricks, and moving average.

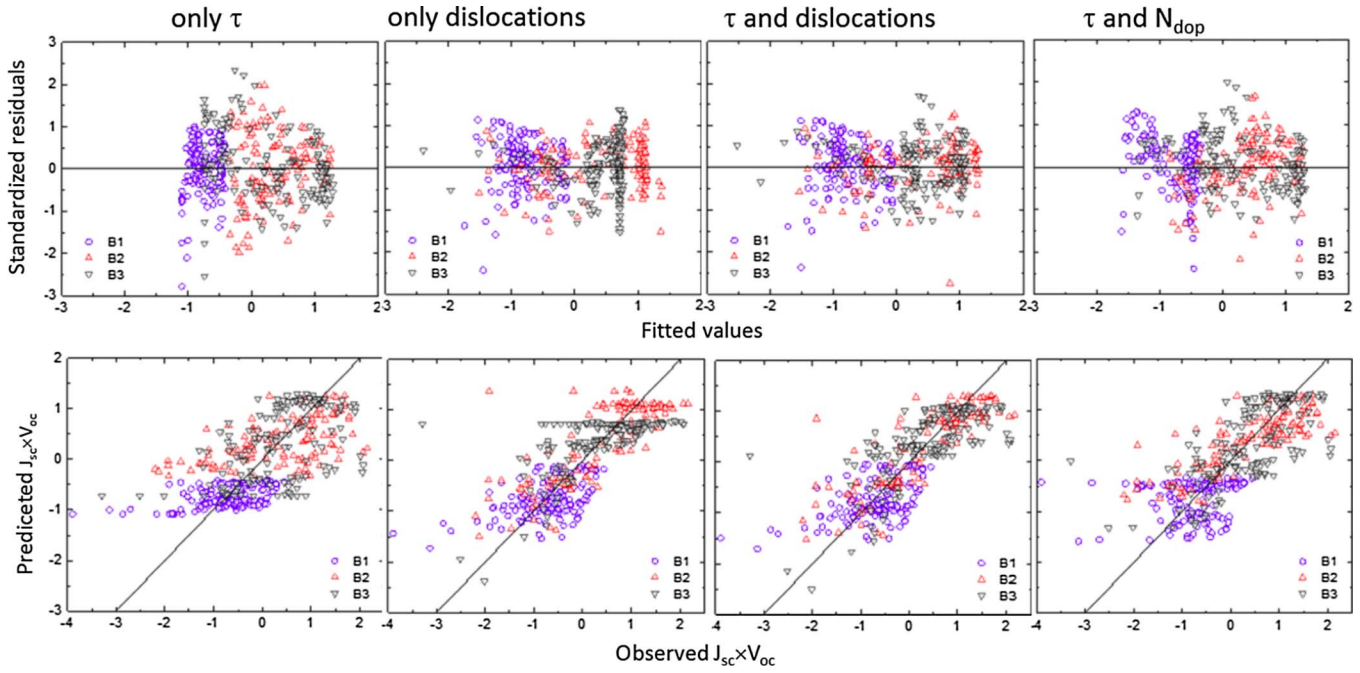

Fig. 8. Mixed linear model used at UNSW for the data evaluation of Fig. 7. Top: standarized errors to the fitted values. Bottom: Predicted vs. observed $J_{sc} \times V_{oc}$.

3. Assessing the quality of multi ingots

Central to multi manufacturing is not only wafer lifetime, but also ingot yield. The lifetime at all sides of exemplary bricks from three different G6 ingots was measured with a line scanning PL imager (BT Imaging LIS-B3) and evaluated at UNSW. The goal is to predict the material related variance of PERC cell efficiency with brick metrology data as reliably as possible. This cannot be done by merely looking at the resulting data in Fig. 7. Instead, a statistical method, called linear mixed modeling, was used. This model is suitable for finding the best

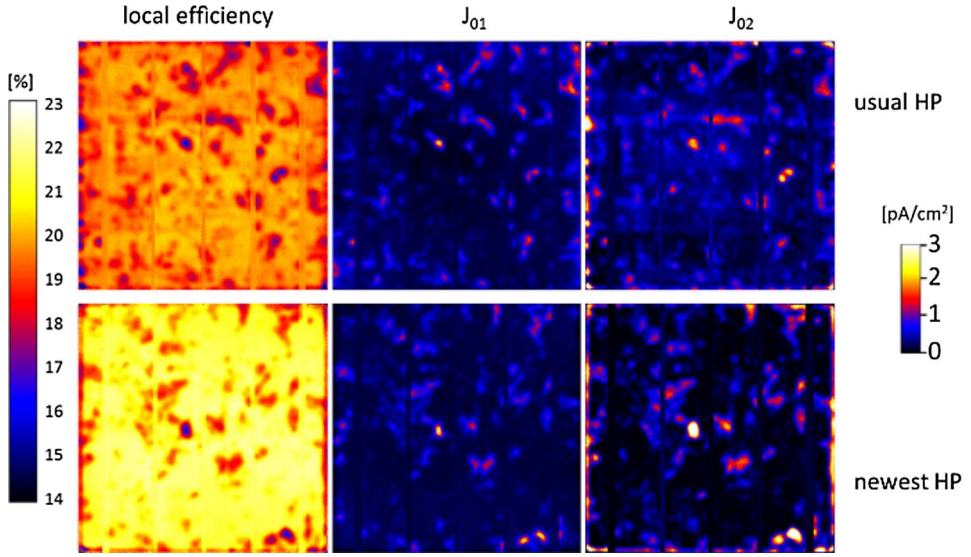

Fig. 9. Spatially resolved assessment of two different PERC cells from Trina, obtained at MPI Microstructure Physics using thermography and the software 'Local IV 2'.

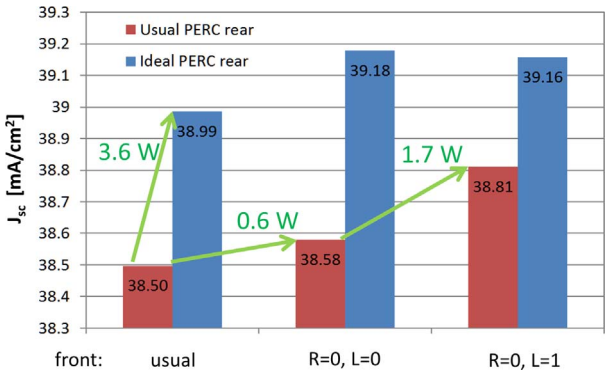

Fig. 10. Ray tracing study, using the Module Ray Tracer from PV Lighthouse, of a multi PERC cell in the module. Left: as usual; middle: zero front surface reflectivity and zero scattering at front; right: with Lambertian scattering at front; red columns for usual PERC cells, blue columns with rear having unity reflectivity and zero absorbance.

predictors when data is statistically fluctuating, includes inter-correlated samples, and is clustering in groups. Modeling revealed that it is best to use both lifetime and a dislocation density parameter to predict PERC cell efficiency, see Fig. 8 for residuals and predicted vs. measured $J_{sc} \times V_{oc}$. Lifetime is only a good predictor for good wafers, where cell processing doesn't dramatically change the wafer lifetime nor dislocations strongly limit the intra-grain lifetime. Adding dislocations into the prediction model helps predicting the material where the intra-grain lifetime is usually limited by a high density of dislocations. Reliable prediction for low efficiencies is crucial, as one likes to discard poor quality wafers before cell production. We chose $J_{sc} \times V_{oc}$ instead of cell efficiency in this case because there were metallization problems in processing the sister wafers in that PERC batch. In routine production, directly cell efficiency can be chosen for predictions. More details are published in reference Mitchell et al. (2017).

4. Assessing multi PERC cells

Fig. 9 shows a spatially resolved assessment of two different PERC cells fabricated at Trina Solar: one from mass production using the usual multi, the other from a pilot line using the newest HP material. The local efficiency, J_{01} (assuming an ideality factor of 1) and J_{02} (ideality factor of 2) are all extracted at the MPI for Microstructure from lock-in thermography images using the method described in reference Breitenstein and Frühauf and using the software 'Local I-V 2'. A central finding comes from the J_{01} image: in finished PERC cells, it is mainly the good areas that have improved in recent material, but the bad areas have remained nearly the same. The efficiency of these cells is mainly dragged down by medium and to some extent by bad areas (the latter are rather small, though). Furthermore, the J_{02} image shows that edge shunts occur. It can be calculated from such plots that cutting off 5 mm of the cell's edge would improve cell efficiency by up to 0.3% absolute at 1-sun, and by up to 1.3% absolute at 0.1-sun. The low-light behavior is particularly important for avoiding mismatch in modules under low light conditions. Furthermore, the slightest contamination due to the transport system in the fabrication shows up in the J_{02} image as well (not shown here). The J_{02} spots in inner cell regions are not shunts, they are caused by a weaker injection-dependence of the lifetime in bad

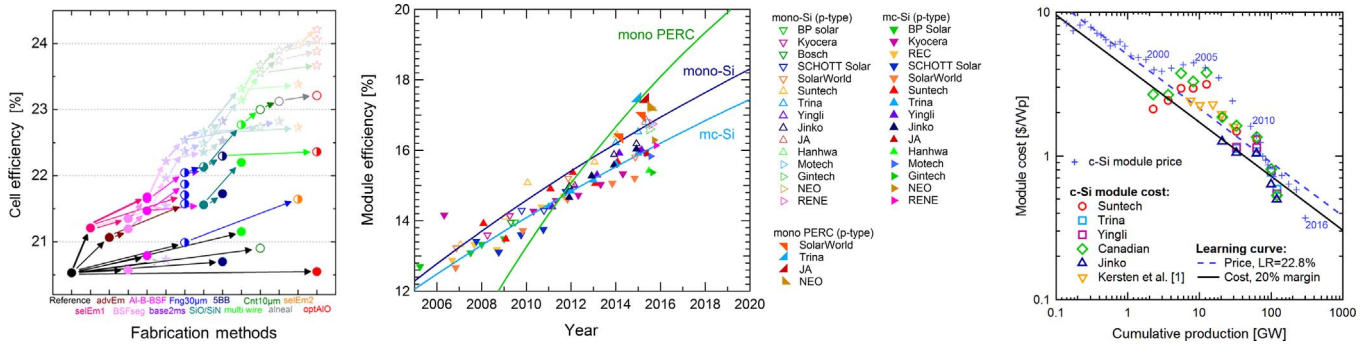

Fig. 11. A PERC roadmap from reference Min et al. (2017) (left), recent evolution of module efficiency (middle) and module cost (right), both from reference Chen et al. (2014).

regions. The robustness of the J_{01} and J_{02} images were tested at MIT by feeding the tiff-files into the software Griddler from SERIS, Singapore, yielding nearly exactly the same IV parameters as were measured with a Sinton FCT-450 flash tester.

Presently, manufacturers are switching their wafering from slurry sawn to diamond-wire sawn techniques to save substantial cost. However, the wafer surfaces after diamond wiring are so smooth that the widely applied acid texturing recipe from the University of Konstanz does not find enough saw damage to be effective. Various texturing methods are presently in intense testing by cell manufacturers, ranging from wafer pre-treatments, additives to chemical etchants, to dry etching or metal assisted processes. In this context, claims of efficiency gains have been made with 'black silicon', meaning that the wafers are etched so thoroughly that they look rather black in air. However, with a ray tracing study, it becomes apparent again that only very small gains can be expected in making silicon 'black' (0.02 mA/cm^2 in J_{sc} or 0.6 W in the module). See Fig. 10. This is so because a good anti-reflection coating (ARC) and total internal reflection at the front glass/air interface are already effective. Some manufacturers choose an ARC so the cells appear dark blue. However, cell appearance can easily be made black by changing the ARC thickness slightly. Hence, it is not necessary to make the silicon appear 'black' in air to obtain black appearance and maximum absorbance in the module. The ray tracing simulations done with the Module Ray Tracer (MRT) from PV Lighthouse indicate, however, that another effect related to texturing can lead to larger gains: if texturing also disperses the light very effectively in all lateral directions when entering the silicon absorption of light is enhanced particularly in its first pass to the back before it is effectively dispersed by the rear surface, having a potential gain of 0.2 mA/cm^2 or 1.7 W (with unity Lambert factor). In contrast, improving the optical properties of the rear surface of PERC cells has a significantly larger potential: increasing the rear reflectance to 1 and removing its parasitic absorbance (mainly at the dielectric/Al interface) would lead to a gain of 0.5 mA/cm^2 and 3.6 W, respectively.

5. Including multi Si material in road maps

Recently, two predictions were made (Data from Energy Trend) based on orders at tool manufacturers: firstly, global PERC fabrication capacity keeps expanding while standard cell production starts to decline. Secondly, the proportion of Si multi decreases from the presently 66% to below 50% next year. This raises the question, to which extend multi material will be used in PERC production in coming years, or whether mono Si will dominate.

Answers to this may be evaluated in two aspects: device physics and economy. Device physics cannot be turned upside down by economy, and thus has its value despite market forces. Reducing J_0 of emitter and rear increases V_{mpp} and thus increases multi lifetime due to $\tau_p = 10\tau_n$ in Fig. 3. Hence, multi lifetime increases with applying higher efficiency cell designs (Wagner et al., 2015) and is therefore conceptually suited for improved cell designs. Still, multi has lower lifetime, thus cell efficiency increments from J_0 improvements are not as strongly felt as in mono material. Therefore, improved cell technologies have tended to be applied first to mono, but soon after also to multi in order to lower production cost. Hence, the above mentioned prediction that mono is going to dominate may be a temporary effect of the presently occurring transition from standard to PERC production.

A further sophisticated guess can be made by comparing the three sub-figures of Fig. 11. The left figure is a PERC roadmap from references Min et al. (2015, 2017), simulated with Sentaurus assuming only already existing technologies for mass fabrication being continually developed further (such as narrower screen-printed fingers, etc). Note that all of the star symbols in the background require 2 ms lifetime at mpp. Hence, multi may become unsuitable for mass production above about 22.5% cell efficiency if the concentrations of Fe_i and Cu remain above 10^{10} and 10^{13} cm^{-3}, respectively, and if dislocations are not reduced further. The middle figure is a projection of the yearly efficiency increase from observations into the future for mass production, taken from reference Chen et al. (2014). According to this, PERC cell efficiency is expected to increase by about 0.4%$_{abs}$ each year in the global market. These two figures combined indicate that in about 8 years PERC cells may come close to 24% cell efficiency (which is about 23% in mass production) and that new technological steps need be introduced every 2nd year to meet that goal. Fabrication cost and module price are, of course, very important for the choice between Cz mono, other mono, quasi-mono, block-cast multi and other multi. Module price fluctuates strongly because a fast growing industry tends to oscillate between demand-limited and fabrication capacity-limited periods. However, the right figure shows the observed module cost in mass production, which fluctuates less than the module price (given by the blue crosses). As margins are rather small, a learning-curve fit to module cost has a similar learning rate as for module price, meaning that after the above-mentioned 8 years, module price may have dropped to half. Hence, economic benefit may keep multi material in production if quality of multi is continuously improved.

This projection of trends from observations in the past into the future assumes that there will be no major market disruptions or technological breakthroughs. With this assumption, hetero-emitters and/or passivated contacts may be incorporated into cell design in mass production in about 8 years or probably earlier. Particularly the hetero-emitter may open a door for other materials than Si to come into the main stream, which may eventually lead to tandem cells containing Si or finally even without Si. Possibly, an earlier shift away from PERC cells may occur if n-type designs become dominant in mass production, such as PERT, bifacial pert, HIT, IBC or others, or if cells made of other materials become cheaper and similarly stable. Also advances in module design may influence the best choice of cell design.

Reference

Breitenstein, O., Frühauf, F. Alternative luminescence image evaluation – comparison with lock-in thermography. Sol. Energy Mater. Sol. Cells (appeared online, doi: http://dx.doi.org/10.1016/j.solmat.2017.06.003).

Chen, Y., Feng, Z., Verlinden, P.J., 2014. Assessment of module efficiency and manufacturing cost for industrial crystalline silicon and thin film technologies. In: Proceedings of the 6th World Conference on PV Energy Conversion, Kyoto, Japan, pp. 1319–1320.

Data from Energy Trend (TrendForce Inc., Taipei, Taiwan), Combined with Data from PV-Tech (Solar Media Ltd., London, UK).

Deng, W., Ye, F., Xiong, Z., Chen, D., Guo, W., Chen, Y., Yang, Y., Altermatt, P.P., Feng, Z., Verlinden, P.J., 2016. Development of high-efficiency industrial p-type multi-crystalline PERC solar cells with efficiency greater than 21%. Energy Procedia 92, 72–729.

Herguth, A., Wilking, S., 2017. CASSANDRA – a tool for analysis and prediction of time resolved BO defect dynamic on lifetime and cell level. Energy Procedia 124, 60–65.

Kwapil, W., Schön, J., Warta, W., Schubert, M., 2015. Carrier recombination at metallic precipitates in p-and n-type silicon. IEEE J. PV 5, 1285–1292 erratum: *ibid* 6 (2016) 391.

Luka, T., Großer, S., Hagendorf, Ch., Ramspeck, K., Turek, M., 2016. Intra-grain versus grain boundary degradation due to illumination and annealing behavior of multi-crystalline solar cells. Sol. Energy Mater. Sol. Cells 158, 43–49.

Min, B., Wagner, H., Müller, M., Neuhaus, H., Brendel, R., Altermatt, P.P., 2015. Incremental efficiency improvements of mass-produced PERC cells up to 24%, predicted solely with continuous development of existing technologies and wafer materials. In: Proceedings of the 31st EU PV Solar Energy Conference, Hamburg, Germany, pp. 473–476.

Min, B., Müller, M., Wagner, H., Fischer, G., Brendel, R., Altermatt, P.P., Neuhaus, H., 2017. A roadmap toward 24% efficient PERC solar cells in industrial mass production. IEEE J. PV 7, 1541–1550.

Mitchell, B., Chung, D., He, Q., Zhang, H., Xiong, Z., Altermatt, P.P., Geelan-Small, P., Trupke, T., 2017. PERC solar cell performance predictions from multicrystalline silicon ingot metrology data. IEEE J. PV 7, 1619–1626.

Needleman, D.B., Wagner, H., Altermatt, P.P., Xiong, Z., Verlinden, P.J., Buonassisi, T., 2016. Dislocation-limited performance of advanced solar cells determined by TCAD modeling. Sol. Energy Mater. Sol. Cells 158, 29–36.

Schmidt, J., Lim, B., Walter, D., Bothe, K., Gatz, S., Dullweber, T., Altermatt, P.P., 2013. Impurity-related limitations of next-generation industrial silicon solar cells. IEEE J. PV 3, 114–118.

Sio, H.C., Phang, S.P., Trupke, T., Macdonald, D., 2014. An accurate method for calibrating photoluminescence-based lifetime images on multi-crystalline silicon wafers. Sol. Energy Mater. Sol. Cells 131, 77–84.

Sperber, D, Graf, A, Skorka, D, Herguth, A, Hahn, G., 2017. Degradation of surface passivation and its impact on light induced degradation experiments. In: Proceedings of the 44th IEEE Photovoltaic Specialists Conference, Washington, DC.
Wagner, H., Hofstetter, J., Mitchell, B., Altermatt, P.P., Buonassisi, T., 2015. Device architecture and lifetime requirements for high efficiency multicrystalline silicon solar cells. Energy Procedia 77, 225–230.
Walter, D.C., Lim, B., Schmidt, J., 2016. Realistic efficiency potential of next-generation industrial Czochralski-grown silicon solar cells after deactivation of the boron–oxygen-related defect center. Prog. PV 24, 920–928.